International Journal of Nanomedicine

Dovepress
open access to scientific and medical research

Open Access Full Text Article

ORIGINAL RESEARCH

Graphene oxide-modified ZnO particles: synthesis, characterization, and antibacterial properties

This article was published in the following Dove Press journal:
International Journal of Nanomedicine
25 August 2015
Number of times this article has been viewed

Linlin Zhong
Kyusik Yun

Department of Bionanotechnology, Gachon University, Gyeonggi-do, Republic of Korea

Abstract: Nanosized ZnO particles with diameters of 15 nm were prepared with a solution precipitation method at low cost and high yield. The synthesis of the particles was functionalized by the organic solvent dimethylformamide, and the particles were covalently bonded to the surface of graphene oxide. The morphology of the graphene oxide sheets and ZnO particles was confirmed with field emission scanning electron microscopy and biological atomic force microscopy. Fourier transform infrared spectroscopy and X-ray diffraction were used to analyze the physical and chemical properties of the ZnO/graphene oxide composites that differed from those of the individual components. Enhanced electrochemical properties were detected with cyclic voltammetry, with a redox peak of the composites at 0.025 mV. Excellent antibacterial activity of ZnO/graphene oxide composites was observed with a microdilution method in which minimum inhibitory concentrations of 6.25 μg/mL for *Escherichia coli* and *Salmonella typhimurium*, 12.5 μg/mL for *Bacillus subtilis*, and 25 μg/mL for *Enterococcus faecalis*. After further study of the antibacterial mechanism, we concluded that a vast number of reactive oxygen species formed on the surface of composites, improving antibacterial properties.

Keywords: graphene oxide, ZnO, characterization, antibacterial property

Introduction

During recent decades, semiconductor nanoparticles have attracted tremendous research attention. In particular, the effect of particle size has been widely studied. The decrease in particle size from the micrometer to the nanometer scale has significantly enhanced the physical, chemical, and biological properties of semiconductor nanoparticles.[1] ZnO is a versatile semiconductor material with wide bandgap (3.37 eV) and large excitation binding energy (60 mV) at room temperature.[2–4] Its properties depend primarily on its extremely large surface area and the number of active surface sites at which reactions occur with absorbed molecules to form hydroxyl and oxide radicals.[5,6] Various ZnO nanoparticle synthesis methods have been developed, including thermal decomposition, sol-gel, and hydrothermal approaches.[7,8] Several new and more convenient methods such as ultrasound, microwave-assisted combustion, and two-step chemical-thermal synthesis have recently been published. Synthesis of ZnO particles with a precipitation method in alcohol solution is the most commonly used and promising low-cost route.[9–11] However, ZnO particles aggregate easily in solution due to van der Waals forces and surface effects.[12] Therefore, the surface of ZnO particles must be modified with an organic reagent or stable polymers to decrease aggregation.[13–15] In this study, we separated ZnO particles by anchoring them on the surface of graphene oxide sheets, thus achieving more stable and dispersed composites.

Correspondence: Kyusik Yun
Department of Bionanotechnology, Gachon University, Gyeonggi-do 13120, Republic of Korea
Tel +82 31 750 8753
Fax +82 31 750 8819
Email ykyusik@gachon.ac.kr

Graphene oxide is a two-dimensional material with intriguing properties such as large surface-to-volume ratio, robust optical transparency, and electronic transport capabilities.[16–18] Microscopic characterization has revealed that graphene oxide has a layered structure in which carbon atoms twist to form tetrahedrons, which creates wrinkles and grooves on the surface.[19] Chemically functionalized groups on the π-conjugated planes of graphene oxide allow easy anchoring of covalently bonded micrometer and nanometer particles onto graphene oxide.[20] Diverse applications for graphene oxide in biological sensors, photocatalysis, and nanocomposites have been explored.[21]

The modification of graphene oxide effectively prevented the aggregation of ZnO particles and resulted in strong stability in the ambient environment.[22] The large surface of graphene oxide and wide bandgap of ZnO particles substantially enhanced the electrochemical properties of the ZnO/graphene oxide composites compared to those of pristine ZnO particles and graphene oxide alone.[23–25] In this study, we examined the antibacterial properties of ZnO/graphene oxide composites with a microdilution method and live/dead assay.[12,26–27] The experimental results showed minimum inhibitory concentrations (MICs) of 6.25 μg/mL for *Escherichia coli* and *Salmonella typhimurium*, 12.5 μg/mL for *Bacillus subtilis*, and 25 μg/mL for *Enterococcus faecalis*. In this study, we demonstrated the antibacterial mechanism of different materials against Gram-positive and Gram-negative bacteria attribute to the production of reactive oxygen species (ROS).[28] The development of ZnO/graphene oxide composites is challenging but significant for applications such as biosensors and antibacterial agents with high efficiency and low toxicity.[29,30]

Materials and methods

Chemicals

Precursor reagents and other chemicals such as graphite powder, zinc acetate, sodium hydroxide, dimethyl sulfoxide (DMSO), 3-aminopropyltriethoxysilane (APTS), and dimethylformamide were commercially obtained from Sigma-Aldrich Co. (St Louis, MO, USA). LIVE/DEAD BacLight kit was used according to manufacturer's protocol (Molecular Probes; Thermo Fisher Scientific, Waltham, MA, USA). Potassium permanganate and hydrogen peroxide were obtained from Junsei Chemical Co., Ltd (Tokyo, Japan). Sulfuric acid and hydrochloric acid were commercially obtained from Daejung Chemicals and Metal Co., Ltd (Gyeonggi-do, Korea). Milli-Q water with a resistance greater than 18 MΩ was used in all experiments. All of the chemicals were of analytical grade and used as received without further purification. Four pathogenic bacterial strains, namely the Gram-negative strains *E. coli* (KACC 10005) and *S. typhimurium* (KCCM 40253), and the Gram-positive strains *B. subtilis* (KACC 14394) and *E. faecalis* (KACC 13807) were utilized in the study. The gold printed circuit board (Au-PCB) working electrode used in the cyclic voltammetry (CV) study was made from a conventional Au printed circuit board (PCB) chip.

Characterization

The ultrasonic system and injection pump used in this study were a VCX 505 Sonics and a KDS101 syringe pump, respectively (KD Scientific, Holliston, MA, USA). Morphological characteristics were studied with a conventional field emission scanning electron microscope (FE-SEM) (JEOL JSM-7500F, 15 kV) and a biological atomic force microscope (Bio-AFM) (NanoWizard II; JPK) in intermittent air mode. Ultraviolet (UV)-visible spectra were analyzed with an Optical 3220. X-ray diffraction (XRD) (Scintag-SDS 2000) was performed at 40 kV voltage and 30 mA current with continuous-scanning 2θ mode. Fourier transform infrared (FT-IR) spectra of the samples were recorded at room temperature with a TENSOR 27 instrument (Bruker) in the 650–4,000 cm^{-1} region. CV measurements were recorded with VersaSTAT 3 (VersaStudio) in a three-electrode configuration. Zetasizer Range (Nano-Z; Malvern Instruments, Malvern, UK) was used for particle size measurement. The stained samples were analyzed using laser scanning fluorescence microscopy (Nikon Eclipse TE 2000-U) and fluorescence-activated cell sorting (FACS) (BD FACSCalibur™; BD Biosciences, San Jose, CA, USA).

Preparation of functionalized ZnO particles

Zinc acetate (0.125 M) and 0.25 M sodium hydroxide solution were dissolved in succession into methanol heated to 65°C under continuous stirring. Then, 10 mL of the sodium hydroxide–methanol solution was collected in a 20 mL syringe and injected into a reaction beaker containing 10 mL zinc acetate. The flow rate was 330 μL/min (maintained by the syringe pump). The solution was stirred at 800 rpm and maintained at a temperature of 65°C.[26]

$$Zn(CH_3CO_2)_2 + 2NaOH \rightarrow Zn(OH)_2 + 2NaCH_3CO_2 \quad (1)$$

$$Zn(OH)_2 \rightarrow ZnO + H_2O \quad (2)$$

An additional 10 mL sodium hydroxide solution was added to the mixture dropwise, and stirring continued for

30 minutes. The resulting white precipitate was separated via centrifugation and washed three times with anhydrous ethanol in an ultrasonication bath. The solution containing ZnO particles was dried in a hot-air oven at 60°C for 24 hours.

Synthesis of graphene oxide sheets

Graphene oxide was synthesized according to the modified Hummer method with graphite powder as a precursor.[27] Graphite powder (2 g) was dissolved in 30 mL sulfuric acid (98%, mass percent) under strong stirring for 1 hour. Potassium permanganate (6 g) was added gradually with stirring, and the solution was kept at 35°C in an ice bath for 1 hour. The mixture was carefully diluted with 100 mL distilled water under vigorous stirring. Subsequently, another 100 mL water and 10 mL 30% hydrogen peroxide solution were added under continuous stirring for 2 hours. The dark brown solution was then filtered and washed with 5% hydrochloric acid solution to remove metal ions. Finally, the suspension was washed by centrifuging with distilled water until the pH of the solution was neutral. Water (100 mL) was added to the purified graphene oxide precipitate, and the mixture was strongly sonicated in a probe-type sonicator for 90 minutes to obtain a uniform graphene oxide solution. The graphene oxide liquid was dried in a hot-air oven at 60°C for 24 hours.

Fabrication of ZnO/graphene oxide composites

The prepared ZnO (0.50 g) was dissolved in 10 mL DMSO and ultrasonicated for 1 hour. APTS (10 mL) was added to the solution and sonicated for 2 hours to complete the reaction. The amino-functionalized ZnO was separated from the solution via centrifugation, washed with absolute ethanol, and dried in an oven. ZnO-APTS particles (0.10 g) and graphene oxide powder were dissolved in dimethylformamide. The solution was mixed and sonicated for 2 hours to obtain uniform dispersion. Finally, ZnO/graphene oxide composites were recovered via centrifugation and washed three times with alcohol, and dried in an oven for future use. Figure 1 shows the fabrication steps briefly.

Electrode pretreatment and immobilization of the product

The surface of the Au-PCB electrode was washed with anhydrous ethanol and deionized water for 3 minutes. Oxygen plasma treatment was then performed on the surface of the Au-PCB electrode for 120 seconds. The graphene oxide and composite liquid (5 µL) was dropped onto the surface of the Au-PCB electrode, and the electrode was left in ambient environment to dry. Finally, the immobilized PCB electrode was coated with 5 µL Nafion. The entire process is shown in Figure 2.

Determination of MIC

E. coli was inoculated into Luria-Bertani broth and cultured overnight at 35°C.[31] To a 96-well plate containing 100 µL of ~10^8 colony-forming units/mL cells was added 100 µL each of ZnO, graphene oxide, and ZnO/graphene oxide composites. The mixtures were incubated at 35°C for 12 hours.

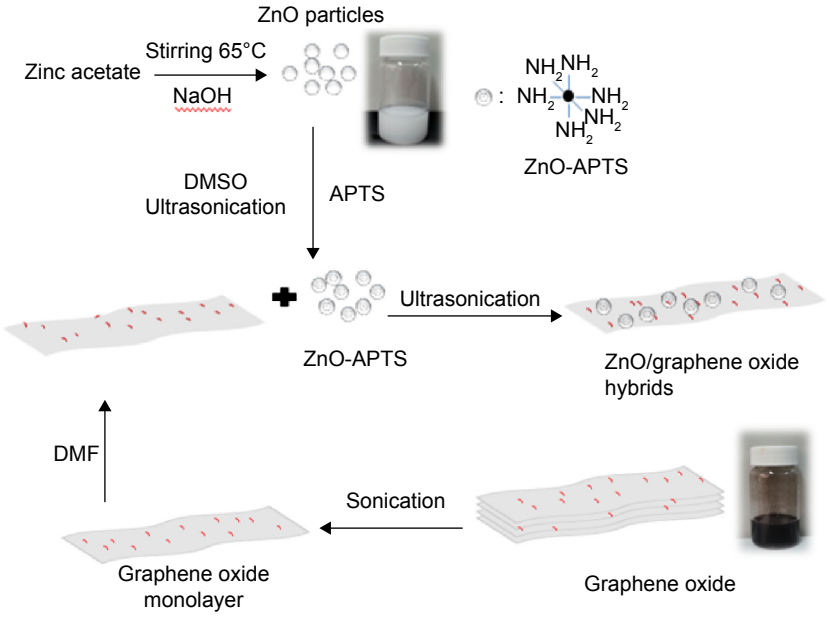

Figure 1 Illustration for the synthesis of the ZnO/graphene oxide composites.
Abbreviations: ZnO, zinc oxide; NaOH, sodium hydroxide; APTS, 3-aminopropyltriethoxysilane; DMSO, dimethyl sulfoxide; DMF, dimethylformamide.

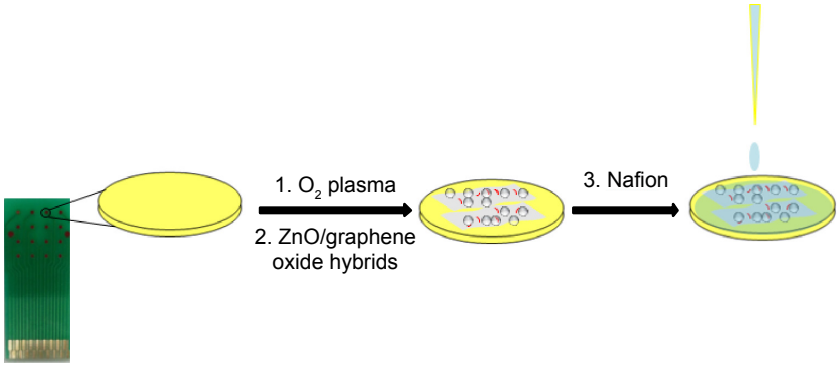

Figure 2 Illustration for the preparation of the Au-PCB/ZnO/graphene oxide platform.
Abbreviations: Au-PCB, gold printed circuit board; ZnO, zinc oxide.

Absorbance in the microwell plates was measured at 590 nm with an enzyme-linked immunosorbent assay reader to confirm the MIC values.

Production of ROS by materials

The production of ROS was determined by the oxidant-sensitive dye 2′,7′-dichlorodihydrofluorescein diacetate (DCFH-DA).[32] For the experiment, a stock solution of 10 Mm DCFH-DA in phosphate buffered saline (pH 7.4) was prepared. Hundred microliters of bacteria (*E. coli*, 108 colony-forming units/mL cells) was mixed with 100 µL different concentrations of ZnO, graphene oxide, and ZnO/graphene oxide composites to incubate for 12 hours at 37°C, and bacteria without sample regarded as contrast. Finally, 100 µL DCFH-DA was added to each well and incubated at room temperature in the dark for 1 hour. Fluorescence intensity was measured to determine the production level of ROS.

Results and discussion

Characterization with FE-SEM and Bio-AFM

Alkaline solution played a key role in this study because Na^+ is attracted to the OH^- around the ZnO core and forms a virtual capping layer to inhibit particle growth.[33] As shown in Figure 3A, ZnO particles ~170 nm in size were uniformly dispersed in the FE-SEM images. The high-magnification FE-SEM image in Figure 3B shows that nanosized ZnO particles assemble to form a round particle. We oxidized graphite to manufacture graphene oxide and exfoliated the graphene oxide monolayer via ultrasonication. Figure 3C shows that the edges of the transparent graphene oxide sheets tended to crimp, and many wrinkles were observed across all of the graphene oxide sheets. Generally, graphene oxide sheets contain unique chemically reactive groups such as carboxyl, hydroxyl, and epoxy groups on their basal planes for covalent reactions.[34] The highly disordered arrangement of the covalently bonded ZnO particles on the graphene oxide sheets is shown in Figure 3D. We detected weight and atomic ratio of C, O, Zn elements of Figure 3D by energy dispersive X-ray spectroscopy. Except coating elements Pt and substrate component Si, no other elements were detected from ZnO/graphene oxide composites. The morphology of the ZnO particles demonstrated on Bio-AFM images is consistent with the FE-SEM micrographs. Figure 4A shows round ZnO particles uniformly dispersed on the substrate. The average size of the ZnO particles is 170 nm, as detected by a Malvern Zetasizer Range. Figure 4B shows the wrinkles and thin grooves on the surface of graphene oxide. The wavy features are much more apparent in the Bio-AFM three-dimensional image. Figure 4C shows unordered ZnO particles anchored on the surface of the graphene oxide sheets. Three-dimensional images show clear morphology in Figure 4D–F.

UV-visible absorbance spectrum

The absorption spectrum of the ZnO particles in the UV-visible range was used to characterize the absorption spectrum related to ZnO semiconductor band structure. As shown in Figure 5, ZnO particles have a strong absorption maximum at a wavelength of 352 nm. Graphene oxide has an absorption peak centered at 235 nm and a shoulder at ~300 nm, which could be assigned to the ð→ð* transition of aromatic C-C bonds and the n→ð* transitions of C=O bonds, respectively.[23] The spectra of the composites show an absorption peak at 352 nm that can be attributed to the absorption of surface-attaching ZnO particles. However, the absorption peak of graphene oxide at 235 nm shifted to 225 nm in the composites. The blueshift of the peak was due to the close conjugation of the ZnO particles and the

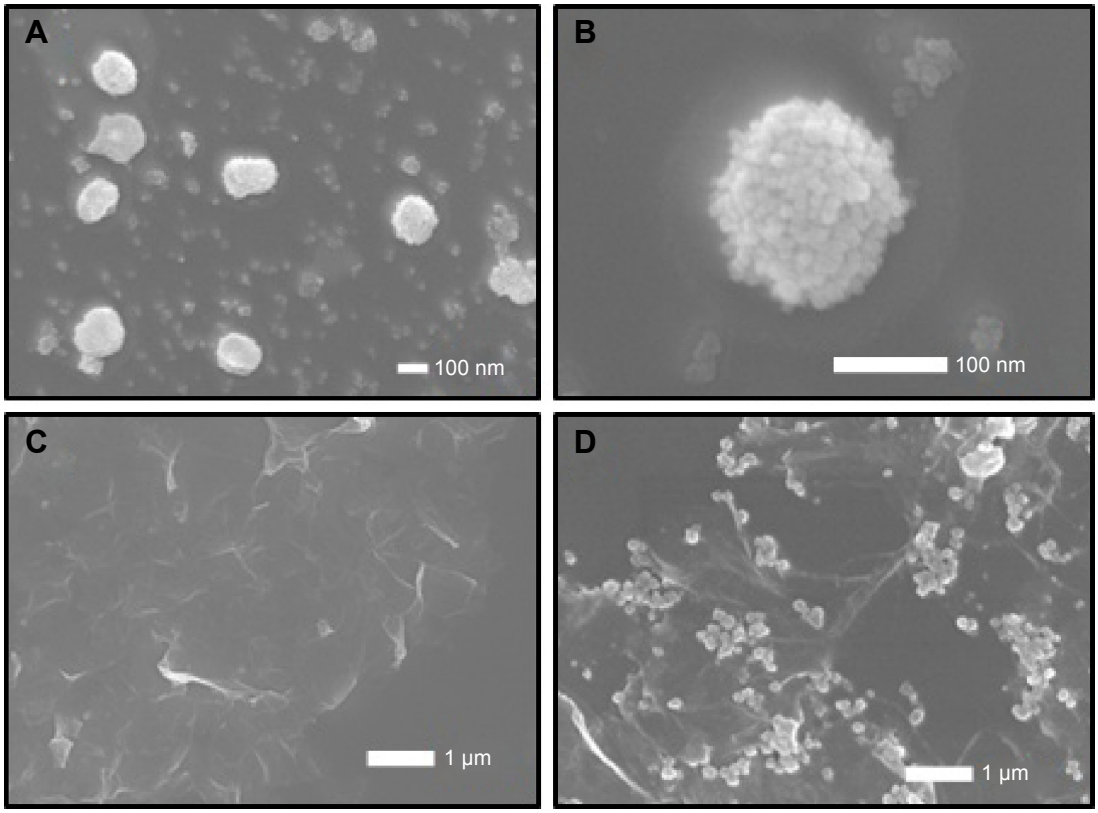

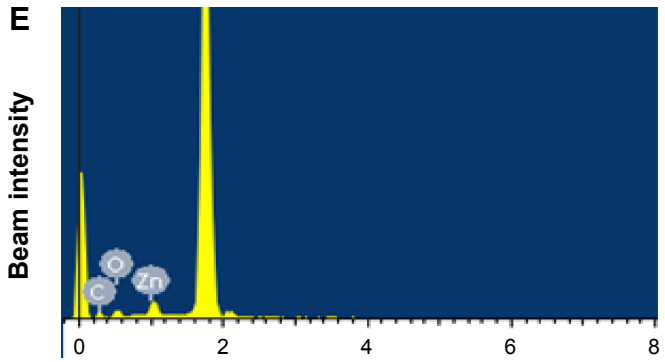

Element	Weight %	Atomic %
CK	33.93	53.83
OK	29.92	35.64
ZnL	36.14	10.54
Totals	100.00	100.00

Figure 3 FE-SEM images and EDX result.
Notes: (**A**) ZnO particles are round in shape and disperse on the substrate; (**B**) a big ZnO particle contains some small nanoparticles; (**C**) graphene oxide has grooves and wrinkles on the edges; (**D**) ZnO particles were anchored onto the surface of graphene oxide via the covalent bonds; (**E**) EDX image clearly show that the sample has pure ZnO phases.
Abbreviations: FE-SEM, field emission scanning electron microscopy; EDX, energy dispersive X-ray spectroscopy; ZnO, zinc oxide.

graphene oxide sheets that resulted in rapid electron transfer and increased transition energy.

X-ray diffraction

XRD is a useful technique for determining interlayer distances and crystalline structure in the powder form of a material by using the Bragg angle. Figure 6A shows the XRD patterns of ZnO powder, including the appearance of characteristic diffraction peaks for pure ZnO particles corresponding to the (100), (002), (101), (102), (110), (103), and (112) planes. All of the diffraction peaks confirm those of crystalline ZnO with a hexagonal wurtzite structure. The sharp diffraction peak observed in Figure 6B for graphene oxide appears at $2\theta = 11.6°$, which agrees with previously reported results.[35] The XRD pattern of the ZnO/graphene oxide composites is identical to that of ZnO in Figure 6C. The disappearance of the (001) reflection of graphene oxide in the XRD pattern of ZnO/graphene oxide composites can be attributed to the intercalation of ZnO particles that damaged the regular stack of graphene oxide.

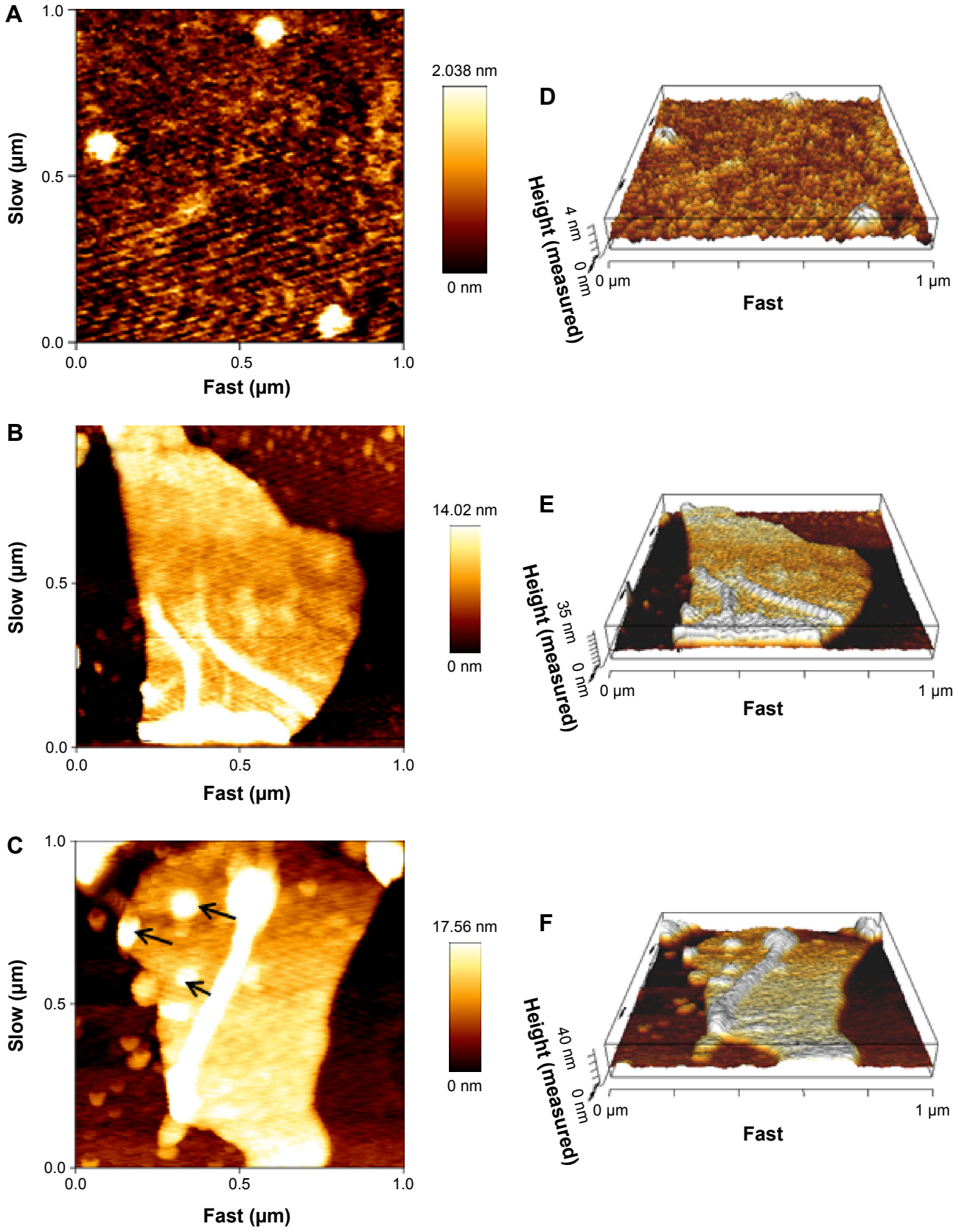

Figure 4 AFM images of ZnO particles, graphene oxide, and ZnO/graphene oxide composites.
Notes: (**A**) ZnO particles were round; (**B**) graphene oxide sheets exhibited some grooves and wrinkles on the surface; (**C**) ZnO particles were anchored onto the surface of graphene oxide sheets. The arrows show the part of ZnO particles and (**D**)–(**F**) are 3D pictures of the three particle parts.
Abbreviations: AFM, atomic force microscopy; ZnO, zinc oxide; 3D, three-dimensional.

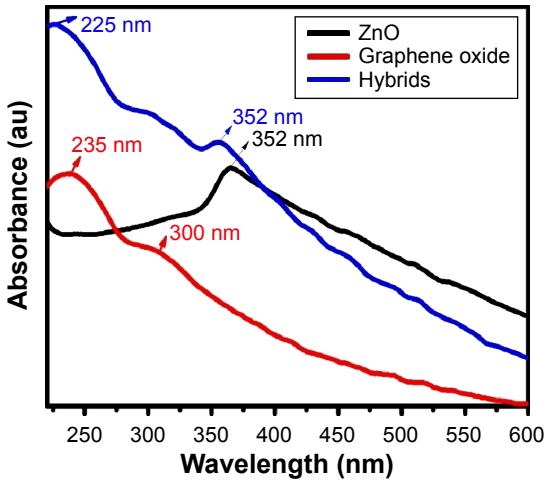

Figure 5 UV-visible absorbance spectra.
Notes: A peak appeared at 352 nm in spectra of ZnO. Graphene oxide exhibited an absorption peak centered at 235 nm and a shoulder at ~300 nm. In composites, one peak appeared at 352 nm related to ZnO, and the other peak corresponding to graphene oxide at 235 nm blueshifts to 225 nm. All peaks in the figure are represented by the correspondingly colored arrows.
Abbreviations: UV, ultraviolet; ZnO, zinc oxide.

FT-IR spectra

The structure analysis of wurtzite ZnO was further supported with FT-IR spectroscopy. The FT-IR peaks of graphene oxide are shown in Figure 7A at 1,050 cm^{-1}, 1,150 cm^{-1}, 1,200 cm^{-1}, 1,450 cm^{-1}, and 3,260 cm^{-1}.[36] The peak at 1,000 cm^{-1} was attributed to C–O vibrations of the graphitic domains. The C–OH group exhibited its peak at 1,150 cm^{-1}. The C=C groups and C=O groups came from carboxylic acid, and their peaks were observed at 1,650 cm^{-1} and 1,750 cm^{-1}, respectively. The peak at 3,350 cm^{-1} was from the O–H groups due to water remaining in graphene oxide. Complete water removal is impossible because graphene oxide absorbs water from the air. Figure 7B shows that the ZnO/graphene oxide composites shared identical peaks with graphene oxide, but a new broad peak was observed at 650 cm^{-1} and was attributed to Zn–O vibrations. These vibrations indicate that ZnO particles were anchored to the graphene oxide sheets.

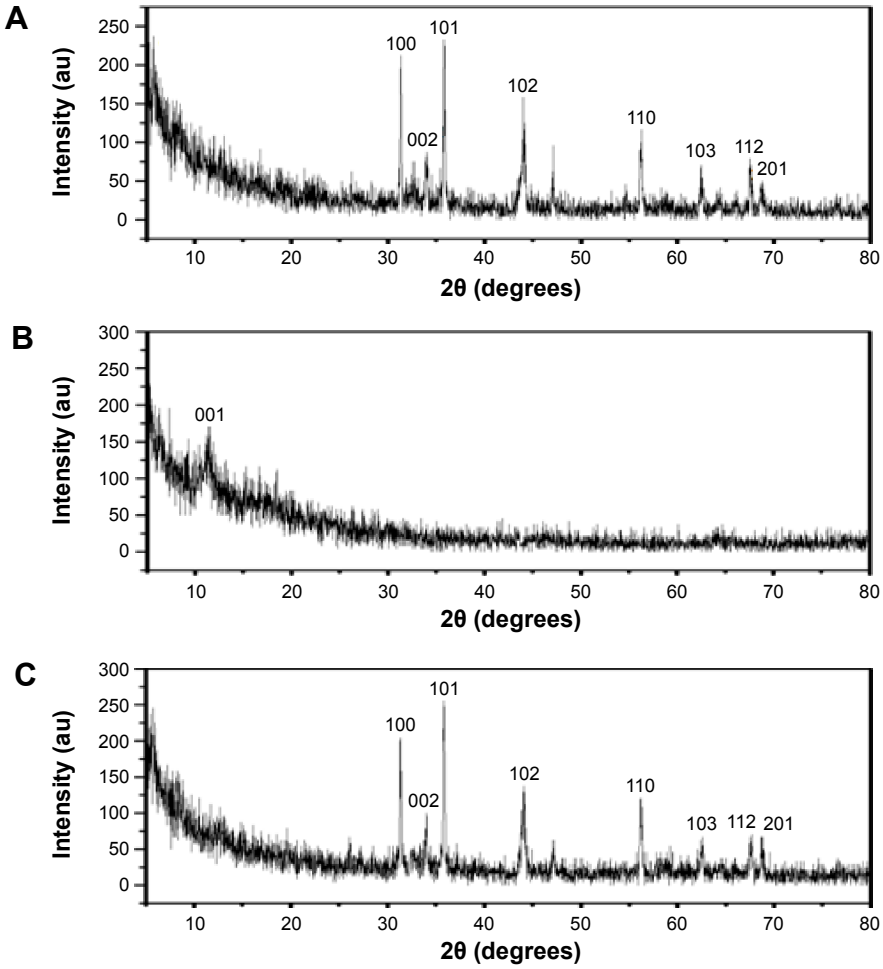

Figure 6 XRD patterns.
Notes: (**A**) ZnO particles; (**B**) graphene oxide; (**C**) ZnO/graphene oxide composites.
Abbreviations: XRD, X-ray diffraction; ZnO, zinc oxide.

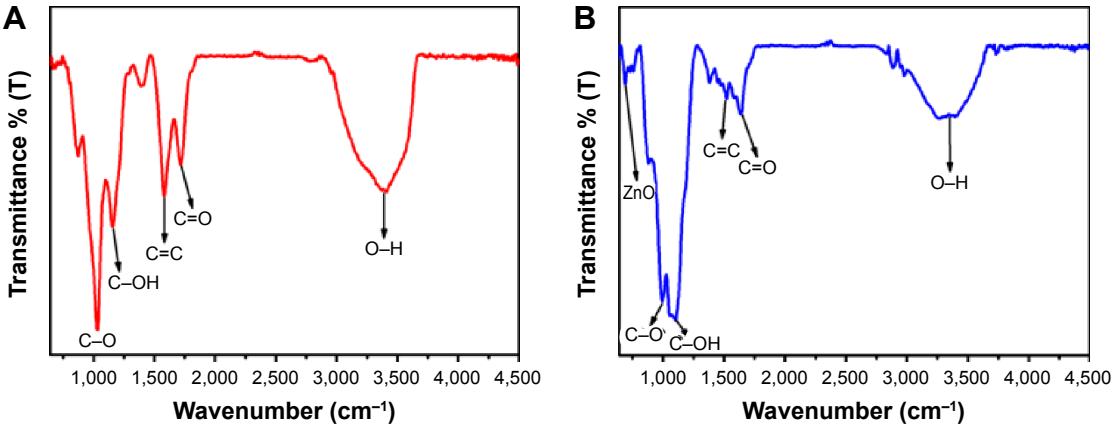

Figure 7 FT-IR spectrum.
Notes: (**A**) the peak of graphene oxide at 1,000 cm^{-1}, 1,150 cm^{-1}, 1,650 cm^{-1}, 1,750 cm^{-1}, and 3,350 cm^{-1} represented C–O, C–OH, C=C, C=O, and O–H, respectively; (**B**) ZnO/graphene oxide composites at 650 cm^{-1}, a special peak attributed to the Zn–O vibration.
Abbreviations: FT-IR, Fourier transform infrared; ZnO, zinc oxide.

Electrochemical measurements

Electrochemical experiments were carried out with a three-electrode cell comprising an Au-PCB working electrode, Pt wire auxiliary electrode, and Ag/AgCl reference electrode. Figure 8A and B shows that no redox peaks appear on the bare Au-PCB and Au-PCB/graphene oxide within a potential range of –0.15 V to +0.25 V at a constant scan rate of 40 mV/s. However, the Au-PCB/ZnO/graphene oxide composites show apparent redox peaks at 0.025 V. We attributed this change to the combination of ZnO particles with graphene oxide via covalent bonds and to robust electron transfer at the redox center of graphene oxide.

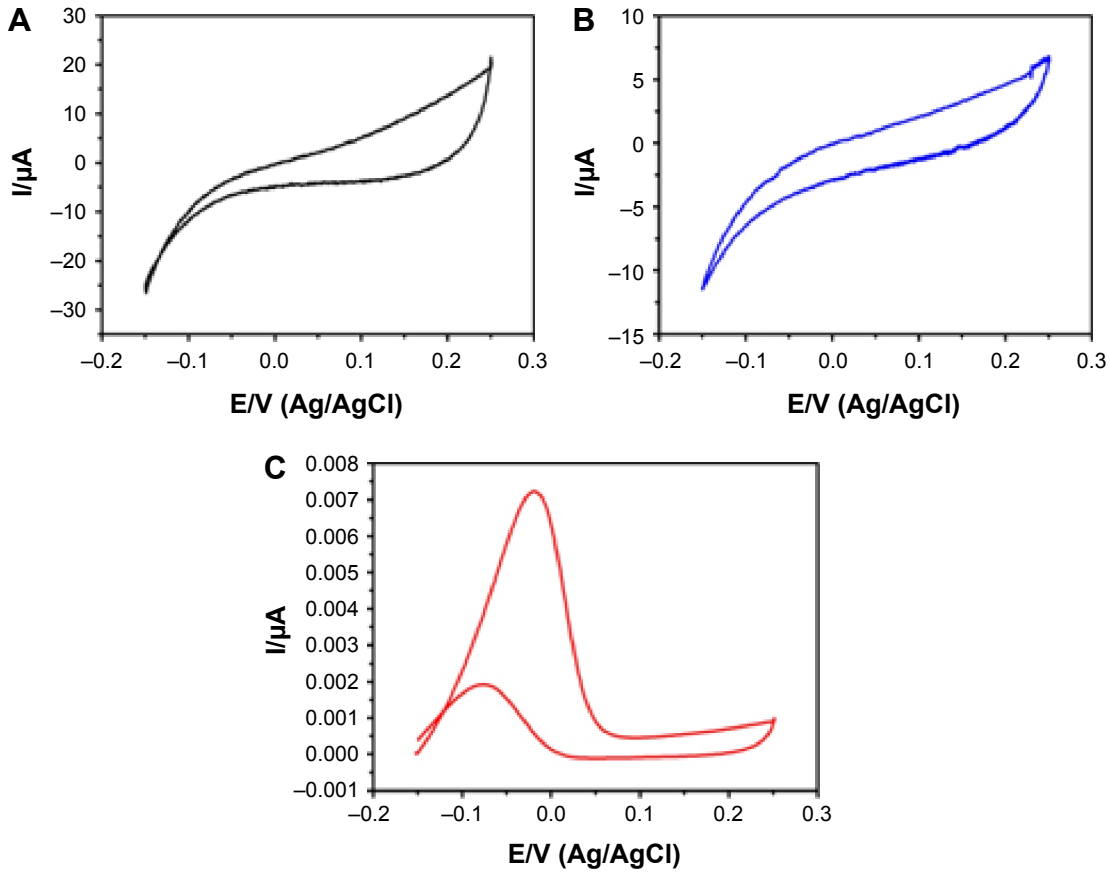

Figure 8 CV curves.
Notes: (**A**) Bare Au-PCB; (**B**) Au-PCB/graphene oxide; (**C**) Au-PCB/ZnO/graphene oxide hybrids.
Abbreviations: CV, cyclic voltammetry; Au-PCB, gold printed circuit board; ZnO, zinc oxide.

Table 1 MIC of samples against Gram-negative and Gram-positive bacterial strains

Bacterial strain	MIC of ZnO (μg/mL)	MIC of GO (μg/mL)	MIC of ZnO/GO (μg/mL)
Escherichia coli	50	12.5	6.25
Salmonella typhimurium	50	12.5	6.25
Bacillus subtilis	100	25	12.5
Enterococcus faecalis	200	50	25

Notes: Experiments were performed in triplicate, and the mean values are reported.
Abbreviations: MIC, minimum inhibitory concentration; ZnO, zinc oxide; GO, graphene oxide.

Antibacterial property analysis with MIC and FACS

A microdilution method and live/dead assay were used to compare the antibacterial activities of ZnO, graphene oxide, and ZnO/graphene oxide composites. MICs for Gram-positive bacteria and Gram-negative bacteria are tabulated in Table 1. MIC value of graphene oxide-Ag is 0.5 mg/mL for *E. coli* and 4 mg/mL for *B. subtilis* have already been reported.[37] Compared to that, the antibacterial property of ZnO/graphene oxide is more remarkable in our work. Representative images of Petri plates with ZnO/graphene oxide composites are shown in Figure 9. The inhibition of bacterial colonies was apparent after incubation for 24 hours. Furthermore, obvious inhibition zones measured in the agar plates through incubation all night are shown in Figure 10; in each disk, 100 μL ZnO/graphene oxide solution of different concentrations was dropped. These prove that ZnO/graphene oxide composites at low concentration can be effectively used to inhibit the growth of bacteria.

SEM images show bacterial morphology under different conditions. Figure 11A demonstrates bacterial growth and membrane integrity without any agents. Figure 11B and C

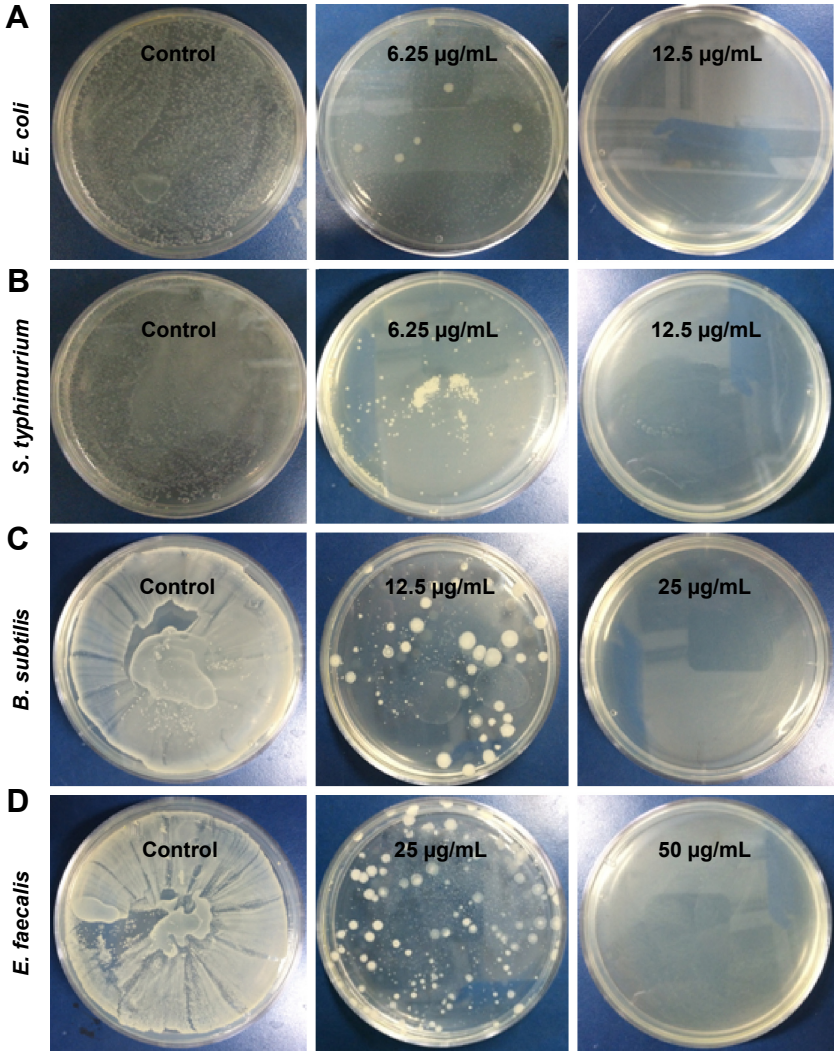

Figure 9 Representative Petri plate images showing the variable number of Gram-negative and Gram-positive bacteria colonies with different amounts of ZnO/graphene oxide.
Notes: (**A**) *Escherichia coli;* (**B**) *Salmonella typhimurium;* (**C**) *Bacillus subtilis;* (**D**) *Enterococcus faecalis.*
Abbreviation: ZnO, zinc oxide.

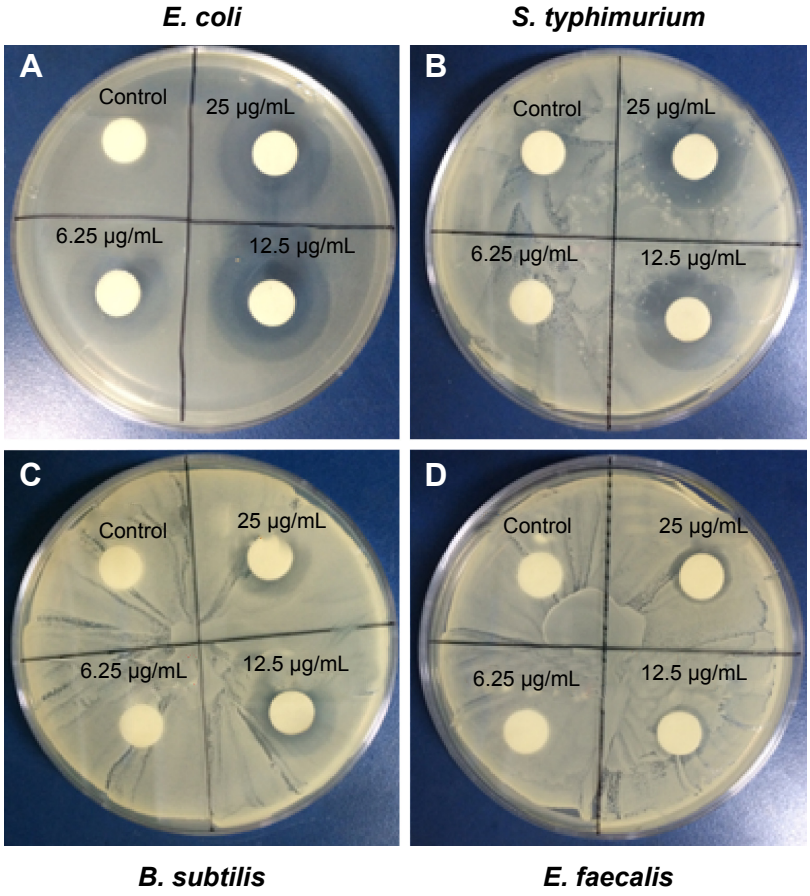

Figure 10 Inhibitory zones of ZnO/graphene oxide composites against (**A**) *Escherichia coli;* (**B**) *Salmonella typhimurium;* (**C**) *Bacillus subtilis;* (**D**) *Enterococcus faecalis.*
Abbreviation: ZnO, zinc oxide.

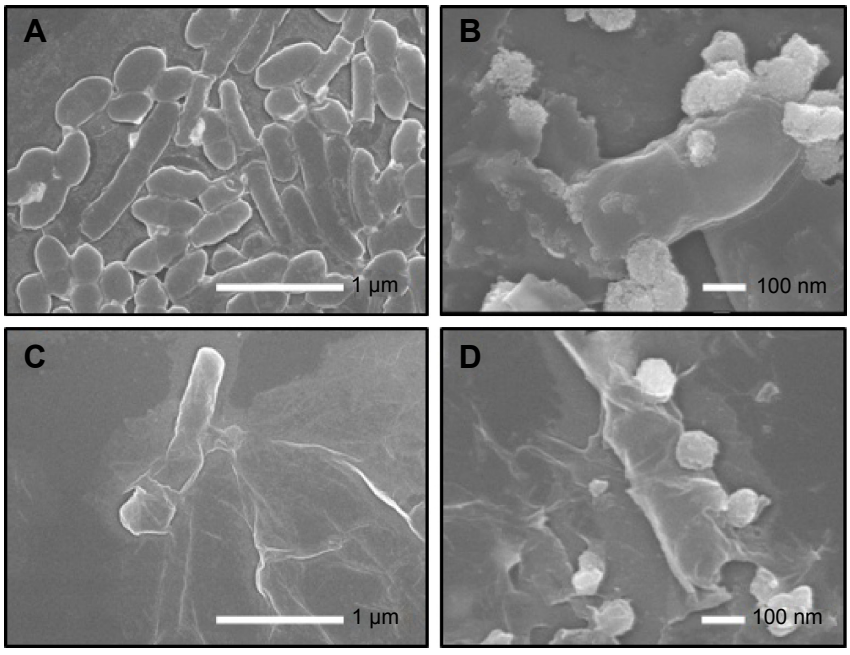

Figure 11 SEM images of (**A**) normal *Escherichia coli* cells with integrated membrane; (**B**)–(**D**) ZnO particles, graphene oxide, and ZnO/graphene oxide composites treated *E. coli*, respectively.
Note: After 2 hours, by comparison, ZnO/graphene oxide composites cause more damage than ZnO particles and graphene oxide sheets.
Abbreviations: SEM, scanning electron microscopy; ZnO, zinc oxide.

shows the destruction of the bacterial surface after 2 hours that is attributed to the antibacterial effects of ZnO particles or graphene oxide sheets because the sides of the bacterial membranes with which they contact are wrinkled. We also observed cytoplasm from destroyed bacteria. Serious damage occurred to bacteria attached to ZnO/graphene oxide composites as shown in Figure 11D, and this result shows that compared with their individual components, ZnO/graphene oxide composites have superior antibacterial activity against *E. coli*.

A summary of the antibacterial mechanisms for ZnO and graphene oxide are as follows: Zn^{2+} connects to the bacterial membrane with a negative charge, combining tightly due to Coulomb forces of attraction.[38] The protein on the membrane solidifies and synthetase is destroyed, causing the bacteria to lose their proliferating capabilities. The antibacterial mechanism for graphene oxide is its special two-dimensional structure that interacts strongly with the bacterial lipid bilayer and causes lipid molecules to separate from the membrane and attach to the graphene oxide sheets. As a result, graphene oxide destroys the bacterial membrane. Given the characteristics of the ZnO/graphene oxide composites, we propose a reasonable explanation for its antibacterial mechanism. Electrons rapidly transfer between the ZnO particles and graphene oxide in the composites. Electrons on graphene oxide can absorb surface oxygen to form various ROS and ultimately lead to the formation of lipid peroxide, damaging the bacterial membrane.

Antibacterial activity of ZnO/graphene oxide is attributed to the production of ROS, including singlet oxygen, hydroxyl radicals, superoxide ions, and hydrogen peroxide. To examine the production of ROS, we used the oxidant-sensing fluorescent probe DCFH-DA. DCFH-DA is a nonpolar dye that converted into the polar derivative DCFH by cellular esterases that are nonfluorescent but switched to highly fluorescent dichlorofluorescein when oxidized by intracellular ROS.[39] The intensity of green fluorescence is proportional to the level of ROS. Figure 12 illustrates the emission spectra of *E. coli* broth incubated with samples after 12 hours, showing the emission peak at 520 nm after excitation at 485 nm. The *E. coli* broth without sample does not show the emission peak at 520 nm. The fluorescent intensity indicates that the ZnO/graphene oxide produced a higher level ROS compared to ZnO and graphene oxide components. Figure 13A displays widespread background green fluorescence, attributing to auto-oxidation by fluorescent microscopy. Figure 13B and C shows weaker green fluorescence, proving ZnO particle

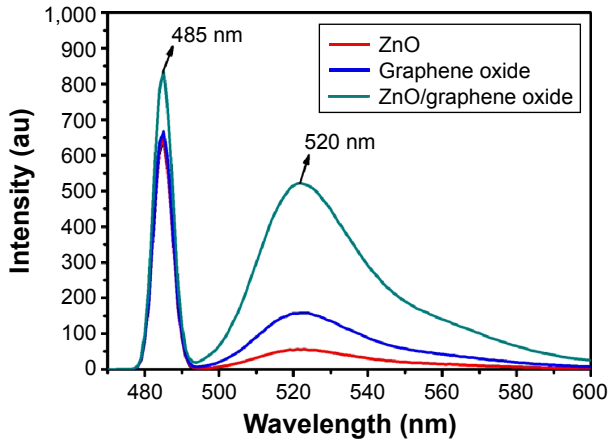

Figure 12 Fluorescence intensity spectra of *Escherichia coli* broth with ZnO, graphene oxide, and ZnO/graphene oxide composites.
Abbreviation: ZnO, zinc oxide.

and graphene oxide components commonly produced low ROS.[39] However, ZnO/graphene oxide composites present noticeable increasing green fluorescence in the *E. coli* cell. According to fluorescence test, we concluded ZnO/graphene oxide composites produced a significant increase in the ROS level.

Representative *E. coli* treated with ZnO, graphene oxide, and the ZnO/graphene oxide composites were separately stained with a LIVE/DEAD BacLight kit according to manufacturer's protocol. After incubation of the bacteria strain with sample for 24 hours, bacteria were washed three times with distilled water. A SYTO 9/propidium iodide mixture strain was dissolved in a mixture of 3% DMSO and double-distilled water; dyed bacteria were then placed in the dark at room temperature for 30 minutes and analyzed with FACS to determine the survival rate. Figure 14 shows dot plots of side scattering intensity versus fluorescence intensity obtained from dead and live *E. coli*. The dead target bacteria dyed with the kit produced red fluorescence signals. By contrast, live bacteria produced bright green fluorescence. Regions representing dead and viable target bacteria were designated P_1 and P_2, respectively. Figure 14A shows strong green fluorescence in the P_2 region, an indication that the majority of the bacteria were alive. A small number of the bacteria were dead due to insufficient nutrition in the media. As observed in Figure 14B and C, more than half of the bacteria were dead, indicating that ZnO particles and graphene oxide sheets possess antibacterial properties. However, Figure 14D shows <20% live bacteria in the P_2 region, an indication that ZnO particles and graphene oxide complement each other to enhance their individual antibacterial activities.

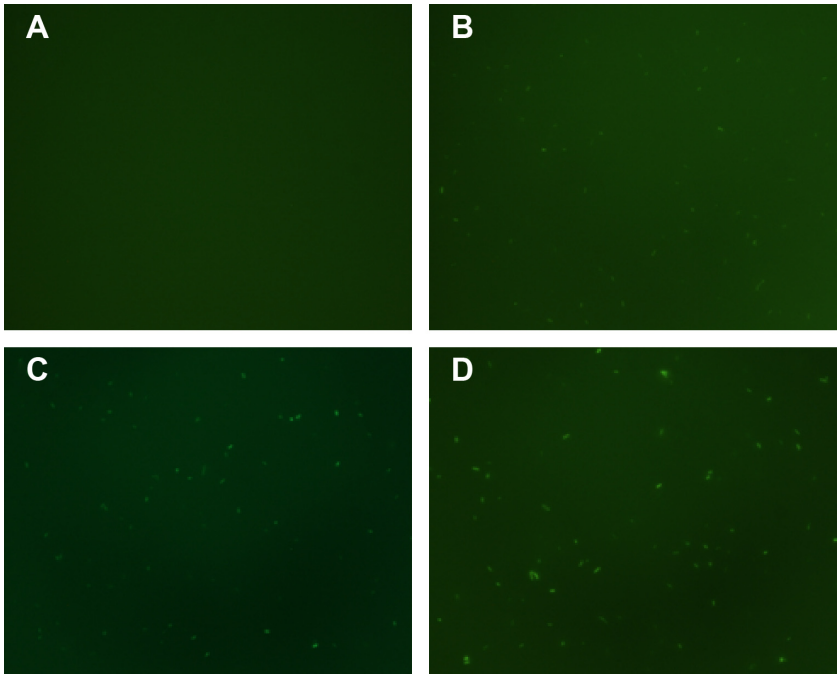

Figure 13 Fluorescence images of *Escherichia coli* cell.
Notes: (**A**) with only DCFH-DA for control; (**B**) with DCFH-DA in ZnO; (**C**) with DCFH-DA in graphene oxide; (**D**) with DCFH-DA in ZnO/graphene oxide.
Abbreviations: DCFH-DA, 2′,7′-dichlorodihydrofluorescein diacetate; ZnO, zinc oxide.

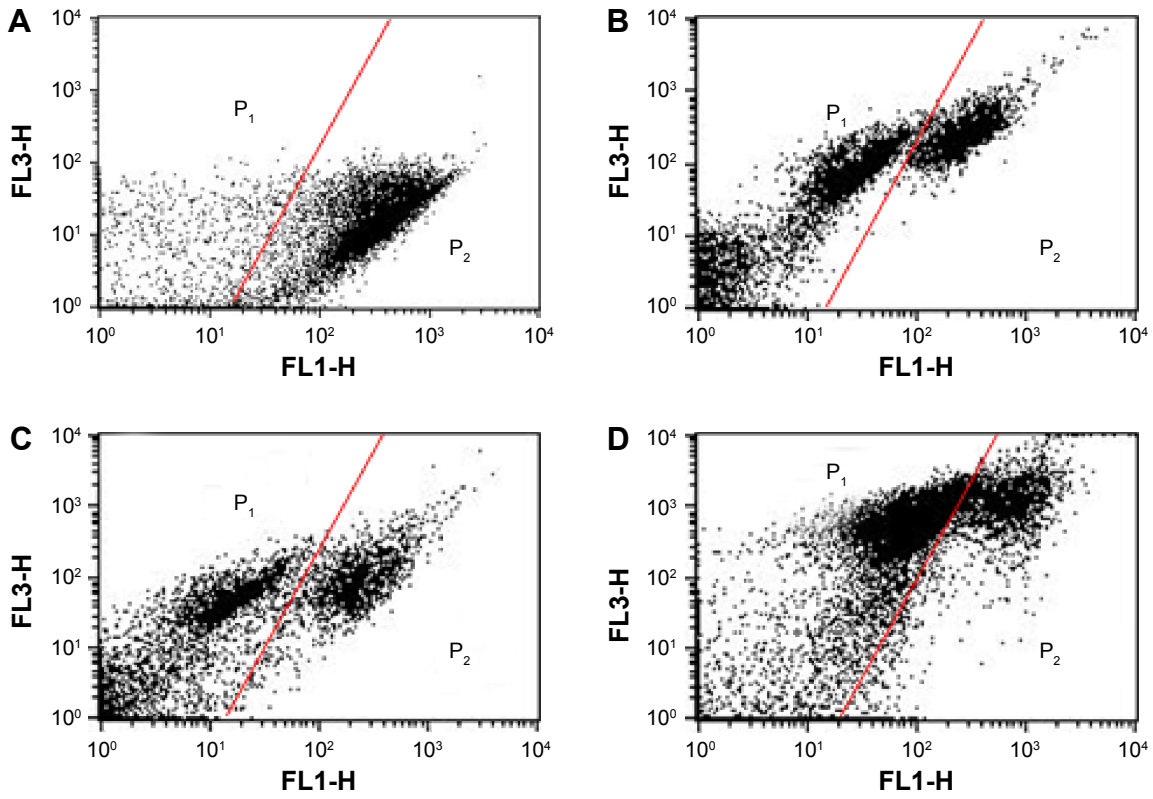

Figure 14 Flow cytometric analysis.
Notes: (**A**) normal *Escherichia coli;* (**B**)–(**D**) *E. coli* were treated with ZnO particles, graphene oxides, and ZnO/graphene oxide composites, respectively. P_1 and P_2 regions stand for dead bacteria and live bacteria. We can estimate antibacterial property through the number of bacteria in P_1 and P_2 regions.
Abbreviation: ZnO, zinc oxide.

Conclusion

We synthesized ZnO particles at low temperature and anchored them to the surface of graphene oxide sheets via a simple and fast method. The synthesized ZnO and graphene oxide were characterized with a UV-visible spectrophotometer and FT-IR spectroscopy. FE-SEM and Bio-AFM images showed the distribution and morphology of ZnO, graphene oxide, and their composites. The size of the ZnO particles was confirmed with a Malvern Zetasizer Range. The electrochemical properties of the composites were detected with CV. The results showed that compared with their individual components, ZnO/graphene oxide composites have enhanced electrochemical properties. The composites also demonstrated excellent antibacterial properties when tested with a microdilution method and live/dead assay, suggesting that they are promising candidates for applications in antibacterial medicine. This cost-efficient method could be adapted to fabricate ZnO/graphene oxide composites suited for super-capacitance, biosensors, and disinfectants.

Acknowledgment

This work was supported by the GRRC program of Gyeonggi Province (GRRC-GACHON2014-B03).

Disclosure

The authors report no competing interests in this work.

References

1. Varsha S, Deepak G, Yogesh CS. Synthesis, characterization and application of zinc oxide nanoparticles (n-ZnO). *Ceram Int*. 2013;39(8):9803–9808.
2. Yang MQ, Xu YJ. Basic principles for observing the photo sensitizer role of graphene in the graphene semiconductor composite photocatalyst from a case study on graphene−ZnO. *J Phys Chem C*. 2013;117(42):21724–21734.
3. Kavitha T, Gopalan AI, Lee KP, Park SY. Glucose sensing, photocatalytic and antibacterial properties of grapheme–ZnO nanoparticle hybrids. *Carbon N Y*. 2012;50(8):2994–3000.
4. Khan Y, Durranib SK, Mehmood M, Ahmad J, Khan MR, Firdous S. Low temperature synthesis of fluorescent ZnO nanoparticles. *Appl Surf Sci*. 2010;257(5):1756–1761.
5. Shi RX, Yang P, Dong XB, Ma Q, Zhang AY. Growth of flower-like ZnO on ZnO nanorod arrays created on zinc substrate through low-temperature hydrothermal synthesis. *Appl Surf Sci*. 2013;264:162–170.
6. Sreetama D, Bichitra NG. Characterization of ZnO nanoparticles grown in presence of folic acid template. *J Nanobiotechnol*. 2012;10:29.
7. Wang YJ, Liu JC, Liu L, Sun DD. Enhancing stability and photocatalytic activity of ZnO nanoparticles by surface modification of graphene oxide. *J Nanosci Nanotechnol*. 2012;12(5):3896–3902.
8. Kumar SS, Venkateswarlu P, Rao VR, Nageswara G, Kumar R. Synthesis, characterization and optical properties of zinc oxide nanoparticles. *Inter Nano Letter*. 2013;3:30.
9. Gu ZJ, Paranthaman P, Xu J, Pan ZW. Aligned ZnO nanorod arrays grown directly on zinc foils and zinc spheres by a low-temperature oxidization method. *ACS Nano*. 2009;3(2):273–278.
10. Luo QP, Yu XY, Lei BX, Chen HY, Kuang DB, Su CY. Reduced graphene oxide-hierarchical ZnO hollow sphere composites with enhanced photocurrent and photocatalytic activity. *J Phys Chem*. 2012;116(14):8111–8117.
11. Moleski R, Leontidis E, Krumeich F. Controlled production of ZnO nanoparticles from zinc glycerolate in a sol–gel silica matrix. *J Colloid Interface Sci*. 2006;302(1):246–253.
12. Goswami N, Sharma DK. Structural and optical properties of unannealed and annealed ZnO nanoparticles prepared by a chemical precipitation technique. *Physica E Low Dimens Syst Nanostruct*. 2010;42(5):1675–1682.
13. Mondal A, Basu R, Das S, Nandy P. Heat induced voltage generation in electrochemical cell containing zinc oxide nanoparticles. *Energy*. 2010;35(5):2160–2163.
14. Hu ZS, Oskam G, Searson PC. Influence of solvent on the growth of ZnO nanoparticles. *J Colloid Interface Sci*. 2003;263(2):454–460.
15. Razali R, Zak AK, Majid WHA, Darroudi M. Solvothermal synthesis of microsphere ZnO nanostructures in DEA media. *Ceram Int*. 2011;37(8):3657–3663.
16. Rather JA, Pilehvar S, Wael KD. A graphene oxide amplification platform tagged with tyrosinase zinc oxide quantum dot hybrids for the electrochemical sensing of hydroxylated polychlorobiphenyls. *Sens Actuators B*. 2014;190:612–620.
17. Krishnamoorthy K, Veerapandian M, Zhang LH, Yun K, Kim SJ. Antibacterial efficiency of graphene nanosheets against pathogenic bacteria via lipid peroxidation. *J Phys Chem*. 2012;116(32):17280–17287.
18. Veerapandian M, Seo Y, Yun KS, Lee MH. Graphene oxide functionalized with silver@silica-polyethylene glycol hybrid nanoparticles for direct electrochemical detection of quercetin. *Biosens. Bioelectron*. 2014;58:200–204.
19. Kapitanova OO, Panin GN, Baranov AN, Kang TW. Synthesis and properties of graphene oxide/graphene nanostructures. *J Korean Phys Soc*. 2012;60(10):1780–1793.
20. Shen J, Yan B, Shi M, Ma H, Li N, Ye M. Synthesis of graphene oxide-based biocomposites through diimide-activated amidation. *J Colloid Interface Sci*. 2011;356(2):543–549.
21. Liu JC, Jeong HS, Liu JZ, et al. Reduction of functionalized graphite oxides by trioctylphosphine in non-polar organic solvents. *Carbon N Y*. 2010;48(8):2282–2289.
22. Veerapandian M, Lee MH, Krishnamoorthy K, Yun K. Synthesis, characterization and electrochemical properties of functionalized graphene oxide. *Carbon N Y*. 2012;50(11):4228–4238.
23. Yang Y, Liu TX. Fabrication and characterization of graphene oxide/zinc oxide nanorods hybrid. *Appli Surf Sci*. 2011;257(21):8950–8954.
24. Zhang LX, Zhao JH, Lu HQ, et al. High sensitive and selective formaldehyde sensors based on nanoparticle-assembled ZnO micro-octahedrons synthesized by homogeneous precipitation method. *Sens Actuator B*. 2011;160(1):364–370.
25. Yu A, Qian JS, Pan H, et al. Micro-lotus constructed by Fe-doped ZnO hierarchically porous nanosheets: preparation, characterization and gas sensing property. *Sens Actuator B*. 2011;158(1):9–16.
26. Chu XF, Zhu XH, Dong YP, Chen TY, Ye MF, Sun WQ. An amperometric glucose biosensor based on the immobilization of glucose oxidase on the platinum electrode modified with NiO doped ZnO nanorods. *J Electroanal Chem*. 2012;676:20–26.
27. Lee DC, Yang HN, Park SH, Kim WJ. Nafion/graphene oxide composite membranes for low humidifying polymer electrolyte membrane fuel cell. *J Menbr Sci*. 2014;452(14):20–28.
28. Ding JJ, Wang MQ, Deng JP, et al. Comparison study between ZnO nanorods coated with graphene oxide and reduced graphene oxide. *J Alloys Compd*. 2013;582:29–32.
29. Ramyadevi J, Jeyasubramanian K, Marikani A, Rajakumar G, Rahuman A. Synthesis and antimicrobial activity of copper nanoparticles. *Mater Lett*. 2012;71:114–116.
30. Smitha SL, Gopchandran KG, Nimisha R, Madhavan K, Ravindran TR. SERS and antibacterial active green synthesized gold nanoparticles. *Plasmonics*. 2012;7(3):515–524.

31. Nanda SS, An SSA, Yi DK. Oxidative stress and antibacterial properties of a graphene oxide-cystamine nanohybrid. *Int J Nanomedicine*. 2015; 10:549–556.
32. Xu S, Wang ZL. One-dimensional ZnO nanostructures: solution growth and functional properties. *Nano Res*. 2011;4(11):1013–1098.
33. Sato M, Harada H, Morito S, et al. Preparation, characterization and properties of novel covalently surface functionalized in oxide nanoparticles. *Appli Surf Sci*. 2010;256(14):4497–4501.
34. Bo Z, Shuai XR, Mao S, et al. Green preparation of reduced graphene oxide for sensing and energy storage applications. *Sci Rep*. 2014;4: 4684.
35. Zhang CC, Chen MX, Xu XY, Zhang L, Zhang L, Xia FL. Graphene oxide reduced and modified by environmentally friendly glycylglycine and its excellent catalytic performance. *Nanotechnology*. 2014;25(13): 135707.
36. Yun H, Kim JD, Choi HC, Lee CW. Antibacterial activity of CNT-Ag and GO-Ag nanocomposites against gram-negative and gram-positive bacteria. *Bull Korean Chem Soc*. 2013;34(11):3261.
37. Kim CS, Nguyen HD, Ignacio RM, Kim JH, Cho HC. Immunotoxicity of zinc oxide nanoparticles with different size and electrostatic charge. *Int J Nanomedicine*. 2014;9(2):195–205.
38. Zeng LZ, Zhou J, Li B, Xing DA. High-sensitivity optical device for the early monitoring of plant pathogen attack via the in vivo detection of ROS bursts. *Front Plant Sci*. 2015;6(99):1–8.
39. Rastogi R, Singh SP, Hader DP, Sinha RP. Detection of reactive oxygen species (ROS) by the oxidant-sensing probe20,70 dichlorodihydrofluorescein diacetate in the cyanobacterium *Anabaena variabilis* PCC 7937. *Biochem Biophys Res Commun*. 2010;397:603–607.